

**Electronic and transport properties of  $n$ -type monolayer black phosphorus at low temperatures**F. W. Han,<sup>1,2</sup> W. Xu,<sup>1,2,3,\*</sup> L. L. Li,<sup>1</sup> C. Zhang,<sup>1</sup> H. M. Dong,<sup>4</sup> and F. M. Peeters<sup>5</sup><sup>1</sup>*Key Laboratory of Materials Physics, Institute of Solid State Physics, Chinese Academy of Sciences, Hefei 230031, China*<sup>2</sup>*University of Science and Technology of China, Hefei 230026, China*<sup>3</sup>*Department of Physics and Astronomy and Yunnan Key Laboratory for Micro/Nano Materials and Technology, Yunnan University, Kunming 650091, China*<sup>4</sup>*School of Physics, China University of Mining and Technology, Xuzhou 221116, China*<sup>5</sup>*Department of Physics, University of Antwerp, Groenenborgerlaan 171, B-2020 Antwerpen, Belgium*

(Received 23 January 2017; published 27 March 2017)

We present a detailed theoretical study of the electronic and transport properties of monolayer black phosphorus (BP). This study is motivated by recent experimental activities in investigating  $n$ -type few-layer BP systems. The electron density of states, the screening length, and the low-temperature electron mobility are calculated for monolayer BP (MLBP). In particular, the electron transport mobilities along the armchair and zigzag directions are examined on the basis of the momentum-balance equation derived from a semiclassical Boltzmann equation. The anisotropic electron mobilities in MLBP along different directions are demonstrated where the electron-impurity scattering is considered. Furthermore, we compare the results obtained from two electronic band structures of MLBP and find that the simplified model can describe quite rightly the electronic and transport properties of MLBP. This study is relevant to the application of few-layer BP based electronic systems as advanced electronic devices.

DOI: [10.1103/PhysRevB.95.115436](https://doi.org/10.1103/PhysRevB.95.115436)**I. INTRODUCTION**

Since the discovery of graphene, the investigation of atomically thin electronic materials has quickly become an important field of research in condensed matter physics and nanoelectronics. These newly developed two-dimensional (2D) materials are often of unique and important electric, optical, mechanical, and thermal properties and have been proposed as advanced materials for a new generation of related devices [1,2]. In particular, black phosphorus (BP) is a recent emerging 2D layered material bonded by the van der Waals force. It is found that BP is one of the thermodynamically more stable phases of phosphorus at ambient temperature and pressure. The presence of the weak van der Waals force can lead the BP to be exfoliated [3] into a few layers and even a monolayer (ML) [4,5]. It has been found that when the thickness of BP decreases from bulk to a few layers and eventually the monolayer, the direct energy gap between the conduction and valence bands increases [7]. For monolayer BP (MLBP), the translational symmetry in the  $z$  direction is broken and a direct energy gap of 1.5–2 eV can be achieved at the  $\Gamma$  point [6] in the electronic band structure. Hence, the few-layer (FL) and ML BP systems are appealing candidates for tunable optoelectronic devices from visible to infrared bandwidth [8]. Moreover, FLBP has been recently demonstrated for potential applications as field-effect transistors (FETs) [6], heterojunction  $p$ - $n$  diodes [9], photovoltaic devices [10], photodetectors [11], etc. Particularly, in MLBP the phosphorus atoms form a hexagonal lattice with a puckered structure due to  $sp^3$  hybridization that can result in an in-plane anisotropic electronic band structure and, thus, in the anisotropic electronic [12], optoelectronic [12], and thermoelectric [13,14] properties.

The previous experimental and theoretical studies have been mainly focused on anisotropic electronic mobility for holes in FLBP and MLBP systems [3,12,15]. One reason is that the anisotropic electronic mobility for holes in these BP systems is larger than that for electrons because the effective mass in the valence band is lighter than that in the conduction band [16,17]. Another reason is mainly due to the fact that it is easier to obtain the  $p$ -type FLBP materials. It was found both experimentally and theoretically [17] that the metastable oxygen absorption on the surface of few-layer BP can lead to  $p$ -type doping upon exposure to air. As a result, relatively high hole density can be achieved in FLBP-based devices and better electronic transport performance (e.g., the mobility) can be observed for holes in FLBP [6,17]. Very recently, the experimental study has been undertaken to observe and measure the anisotropic electronic mobility for electrons in  $n$ -type FLBP [17]. For the time being, less theoretical study on electronic and transport properties of  $n$ -type FL and ML BP has been carried out. In conjunction with very recent experimental work on investigating  $n$ -type FLBP, here we would like to conduct a theoretical study in understanding the basic electronic and transport properties of electrons in MLBP.

From a viewpoint of theoretical study, it is desirable and significant to be able to develop the simple and tractable approach in order to save CPU time and to obtain more transparent and understandable theoretical findings. In the present study, we intend to compare the results obtained from two band structure calculations. We would like to figure out a simplified model for further and more complicated calculations. The paper is organized as follows. The electronic band structure, the electron density of states, the Fermi level, the screening length, and the electron transport mobility in  $n$ -type MLBP are investigated in Sec. II. In Sec. III, we present the numerical results and detailed discussions on electronic and transport properties of MLBP. The concluding remarks from this study are summarized in Sec. IV.

\*wenxu\_issp@aliyun.com

## II. THEORETIC APPROACH

### A. Hamiltonian

The Hamiltonian to describe a carrier in MLBP can be obtained from the  $\mathbf{k} \cdot \mathbf{p}$  band structure calculation, which is proposed as [18]

$$H_0 = \begin{bmatrix} E_c + \alpha_c k_x^2 + \beta_c k_y^2 & \gamma k_x \\ \gamma k_x & E_v - \alpha_v k_x^2 - \beta_v k_y^2 \end{bmatrix}, \quad (1)$$

where  $\mathbf{k} = (k_x, k_y)$  is the in-plane electronic wave vector or momentum operator,  $E_c$  and  $E_v$  are respectively the conduction and valence band edge energies,  $E_g = E_c - E_v$  is the band gap,  $\alpha_{c/v}$  and  $\beta_{c/v}$  are parameters for the conduction/valence band, and  $\gamma$  describes the effective coupling strength between the conduction and valence bands. By solving the corresponding Schrödinger equation, the analytical expression of the eigenvalue and eigenfunction for a free carrier in MLBP are obtained, respectively, as [19]

$$E_{\pm}(\mathbf{k}) = [h_c + h_v \pm \sqrt{(h_c - h_v)^2 + 4|h_{cv}|^2}]/2 \quad (2)$$

and

$$\Psi_{\mathbf{k}\pm}(\mathbf{r}) = \frac{h_{cv}}{\sqrt{(E_{\pm} - h_c)^2 + h_{cv}^2}} \begin{bmatrix} 1 \\ (E_{\pm} - h_c)/h_{cv} \end{bmatrix} e^{i\mathbf{k}\cdot\mathbf{r}}, \quad (3)$$

where  $\mathbf{r} = (x, y)$ ,  $h_c = E_c + \alpha_c k_x^2 + \beta_c k_y^2$ ,  $h_v = E_v - \alpha_v k_x^2 - \beta_v k_y^2$ ,  $h_{cv} = \gamma k_x$ , and the upper (lower) case refers to the conduction (valence) band. In this study, we choose the  $x$  axis as the armchair direction and the  $y$  axis as the zigzag direction of the MLBP system.

For the case of a small  $\mathbf{k}$ , we have  $(h_c - h_v)^2 \approx E_g^2 \gg 4|h_{cv}|^2$  so that

$$E_{\pm}(\mathbf{k}) \simeq h_{c/v} \pm \gamma^2 k_x^2 / E_g = E_{c/v} \pm \frac{\hbar^2 k_x^2}{2m_{xc/v}} \pm \frac{\hbar^2 k_y^2}{2m_{yc/v}}, \quad (4)$$

which is much simpler than Eq. (2) from an analytical point of view. Here  $m_{xc/v}$  and  $m_{yc/v}$  are respectively the effective electron masses in the conduction/valence band along different directions. It should be noted that the band parameters  $\alpha_{c/v}$  and  $\beta_{c/v}$  are related to the effective electron masses along different directions via [18]

$$m_{xc/v} = \hbar^2 / [2(\alpha_{c/v} + \gamma^2 / E_g)] \quad (5)$$

and

$$m_{yc/v} = \hbar^2 / (2\beta_{c/v}). \quad (6)$$

In order to see more clearly and to compare the theoretical results obtained from different electronic energy spectra given by Eq. (2) and Eq. (4), from now on we denote Eq. (2) as model I and Eq. (4) as model II. We would like to examine how these two models for different electronic energy spectra affect the electronic and transport properties of MLBP.

### B. The electronic density of states

The Green's function for a free electron in an electronic system is defined as  $G_{\pm}(E) = P(1/[E - E_{\pm}(\mathbf{k})]) - i\pi\delta[E - E_{\pm}(\mathbf{k})]$ , with  $P$  being the principal value and  $E$  the electron energy. From now on, we discuss the case for an electron in

the conduction band in MLBP and take the reference energy from the bottom of the conduction band (i.e., take  $E_c = 0$ ). The density of states (DOS) for an electron can be obtained from the imaginary part of the Green's function, which reads

$$D_+(E) = -\frac{g_s}{\pi} \sum_{\mathbf{k}} \text{Im}G_+(E) \\ = \frac{g_s}{(2\pi)^2} \Theta(E) \sum_i \int_0^{2\pi} d\phi \frac{k_i(\phi)}{|\partial h(k, \phi) / \partial k|_{k=k_i}}, \quad (7)$$

where  $\Theta(E)$  is a unit step function,  $g_s = 2$  counts for spin degeneracy, and  $k_i(\phi)$  is the  $i$ th solution for  $k$  from the equation  $h(k, \phi) = E - E_+(\mathbf{k}) = 0$  with  $\phi$  being the angle between  $\mathbf{k}$  and the  $x$  direction. Here, we carry out the calculation for model I in the polar coordinates. The details about the derivation of  $\partial h(k, \phi) / \partial k$  for model I are presented in the Appendix. For the case of a small  $\mathbf{k}$ , the electronic DOS from model II is simply given as  $D_+(E) = D_0 \Theta(E)$ , where  $D_0 = m_d / \pi \hbar^2$  and  $m_d = \sqrt{m_{xc} m_{yc}}$  is the DOS effective electron mass. The DOS for electrons obtained from model II for MLBP is similar to that for a semiconductor-based 2D electron gas (2DEG) with a parabolic subband structure.

### C. The Fermi level

With the electronic DOS, we can determine the Fermi level in an electronic system by applying the condition of electron number conservation:  $n_e = g_s \sum_{\mathbf{k}} f[E_+(\mathbf{k})]$  with  $n_e$  being the electron density,  $f(x) = [e^{(x - E_F)/k_B T} + 1]^{-1}$  being the Fermi-Dirac function, and  $E_F$  the chemical potential (or Fermi energy at low temperatures). For the case of electrons in MLBP, at the low-temperature limit  $T \rightarrow 0$ , we have  $f(x) \rightarrow \Theta(E_F - x)$  and

$$n_e = \frac{1}{(2\pi)^2} \int_0^{2\pi} d\phi k_i^2(\phi), \quad (8)$$

where  $k_i(\phi)$  is the solution for  $k$  from the equation  $E_F - E_+(\mathbf{k}) = 0$ , which is similar to the case of calculating the DOS (see the Appendix). For the case of the electronic band structure given by Eq. (2) (i.e., model I), Eq. (8) can only be solved numerically. For the case of electronic band structure given by Eq. (4) (model II), we can get an analytical expression for the Fermi level as  $E_F = n_e \pi \hbar^2 / m_d = \hbar^2 k_F^2 / 2m_d$  with  $k_F = \sqrt{2\pi n_e}$  being the Fermi wave vector. The Fermi level for electrons obtained from model II for MLBP is similar to that for a semiconductor-based 2DEG with a parabolic subband structure.

### D. The random phase approximation screening length

With the electron wave function, we can calculate the electrostatic energy induced by the bare electron-electron (e-e) interaction, which reads

$$V_0(\mathbf{k}, \mathbf{q}) = V(\mathbf{k} + \mathbf{q}, \mathbf{k} - \mathbf{q}, \mathbf{k}), \quad (9)$$

with

$$V(\mathbf{k}'_1, \mathbf{k}_1, \mathbf{k}'_2, \mathbf{k}_2) = \int d^2\mathbf{r}_1 d^2\mathbf{r}_2 \Psi_{\mathbf{k}'_1+}^*(\mathbf{r}_1) \Psi_{\mathbf{k}_1+}(\mathbf{r}_1) \\ \times \frac{e^2}{\kappa |\mathbf{r}_1 - \mathbf{r}_2|} \Psi_{\mathbf{k}'_2+}^*(\mathbf{r}_2) \Psi_{\mathbf{k}_2+}(\mathbf{r}_2) \\ = F_0(\mathbf{k}, \mathbf{q}) V_q,$$

where the momentum conservation law has been applied [20]. Here,  $V_q = 2\pi e^2/\kappa q$  is the Fourier transformation of the Coulomb potential with  $\kappa$  being the static dielectric constant of MLBP,  $\mathbf{q} = (q_x, q_y)$  is the change of the electron wave vector during an e-e interaction event, and  $F_0(\mathbf{k}, \mathbf{q}) = \langle \mathbf{k} + \mathbf{q} | \mathbf{k} \rangle \langle \mathbf{k} - \mathbf{q} | \mathbf{k} \rangle$  is the product of the electron wave functions. The strength of the effective e-e interaction can be calculated through  $V_{\text{eff}} = \varepsilon^{-1}(\Omega, \mathbf{q}) V_0(\mathbf{k}, \mathbf{q})$ , where  $\varepsilon(\Omega, \mathbf{q})$  is the dynamical dielectric function matrix with  $\Omega$  being the excitation frequency. Under the random phase approximation (RPA) the dielectric function matrix is written as

$$\varepsilon(\Omega, \mathbf{q}) = 1 - \sum_{\mathbf{k}} V_0(\mathbf{k}, \mathbf{q}) \Pi(\Omega; \mathbf{k}, \mathbf{q}) \quad (10)$$

and

$$\Pi(\Omega; \mathbf{k}, \mathbf{q}) = g_s \frac{f[E_+(\mathbf{k} + \mathbf{q})] - f[E_+(\mathbf{k})]}{\hbar\Omega + E_+(\mathbf{k} + \mathbf{q}) - E_+(\mathbf{k}) + i\delta}$$

is the pair bubble or density-density correlation function. Here  $f(x)$  is the Fermi-Dirac function. At a long-wavelength limit  $q \rightarrow 0$ ,  $F_0(\mathbf{k}, \mathbf{q}) \simeq 1$  and  $V_0(\mathbf{k}, \mathbf{q}) \simeq V_q$ . For a static case  $\Omega = 0$  and at the  $T \rightarrow 0$  and  $q \rightarrow 0$  limits, the real part of the pair bubble becomes

$$\begin{aligned} & \lim_{q \rightarrow 0} \sum_{\mathbf{k}} \text{Re} \Pi(0; \mathbf{k}, \mathbf{q}) \\ &= \eta = -\frac{g_s}{(2\pi)^2} \sum_i \int_0^{2\pi} d\phi \frac{k_i(\phi)}{|\partial h(k, \phi)/\partial k|_{k=k_i}}, \quad (11) \end{aligned}$$

where  $k_i(\phi)$  is the  $i$ th solution for  $k$  from equation  $h(k, \phi) = E_F - E_+(\mathbf{k}) = 0$ . At a low-temperature limit, the equation  $df(x)/dx = -\delta(E_F - x)$  has been applied to derive Eq. (11). Thus, the real part of the static dielectric function can be written as  $\text{Re} \varepsilon(0, \mathbf{q}) = 1 + K_s(\mathbf{q})/q$  with  $K_s(\mathbf{q}) = -(2\pi e^2/\kappa) \sum_{\mathbf{k}} \text{Re} \Pi(0; \mathbf{k}, \mathbf{q})$  being the inverse

screening length. At the  $T \rightarrow 0$  and  $q \rightarrow 0$  limits, we have

$$K_s(\mathbf{q}) \rightarrow K_s = -\frac{2\pi e^2 \eta}{\kappa}. \quad (12)$$

For the case of model I,  $K_s$  can only be determined numerically using Eq. (11). For the case of model II, we have  $\lim_{q \rightarrow 0} \sum_{\mathbf{k}} \text{Re} \Pi(0; \mathbf{k}, \mathbf{q}) = -m_d/\pi\hbar^2 = -D_0$  and the inverse screening length is simply  $K_s = 2\pi e^2 D_0/\kappa$ . Such a result is in line with that published previously [15,21].

### E. The electron-impurity scattering

At relatively low-temperatures, the electron-impurity (e-i) scattering is the principle channel for relaxation of electrons in an electronic system. For the case where the e-i scattering is achieved through the Coulomb potential induced by charged impurities that are three-dimensional-like, the e-i interaction Hamiltonian is given as [20]

$$H_{e-i} = \frac{e^2}{\kappa_I} \frac{1}{|\mathbf{R} - \mathbf{R}_a|}, \quad (13)$$

where  $\mathbf{R} = (\mathbf{r}, 0)$  is the coordinate of an electron in MLBP, the impurity is located at  $\mathbf{R}_a = (\mathbf{r}_a, z_a) = (x_a, y_a, z_a)$ , and  $\kappa_I$  is the static dielectric constant of the medium that contains the impurities. After assuming that the system can be separated into the electrons of interest  $|\mathbf{k}\rangle$  and the rest of impurities  $|I\rangle$ , namely  $|\mathbf{k}; I\rangle = |\mathbf{k}\rangle|I\rangle$ , the e-i interaction matrix element is obtained, in the absence of e-e screening, as [20]

$$\begin{aligned} U(q, \mathbf{R}_a) &= \langle \mathbf{k}'; I | H_{e-i} | \mathbf{k}; I \rangle \\ &= \langle \mathbf{k}' | \mathbf{k} \rangle \frac{2\pi e^2}{\kappa_I q} e^{-q|z_a|} \sqrt{n_i(z_a)} e^{-i\mathbf{q}\cdot\mathbf{r}_a} \delta_{\mathbf{k}', \mathbf{k}+\mathbf{q}}, \quad (14) \end{aligned}$$

where  $\langle I' | I \rangle = \sqrt{n_i(z_a)}$  with  $n_i(z)$  being the impurity distribution along the  $z$  direction,  $\mathbf{q} = (q_x, q_y)$  being the change of the electron wave vector during a scattering event, and

$$\langle \mathbf{k}' | \mathbf{k} \rangle = \frac{[E_+(\mathbf{k}') - h_c(\mathbf{k}')] [E_+(\mathbf{k}) - h_c(\mathbf{k})] + h_{cv}(\mathbf{k}') h_{cv}(\mathbf{k})}{\sqrt{[E_+(\mathbf{k}') - h_c(\mathbf{k}')]^2 + h_{cv}^2(\mathbf{k}')} \sqrt{[E_+(\mathbf{k}) - h_c(\mathbf{k})]^2 + h_{cv}^2(\mathbf{k})}}.$$

Here, we have assumed that the impurities are distributed uniformly along the  $xy$  plane. Using Fermi's golden rule, the electronic transition rate for scattering of an electron from a state  $|\mathbf{k}\rangle$  to a state  $|\mathbf{k}'\rangle$  due to e-i interaction is obtained in the presence of e-e screening as [20]

$$W(\mathbf{k}', \mathbf{k}) = \frac{2\pi}{\hbar} |U_q|^2 F(\mathbf{k}', \mathbf{k}) \delta_{\mathbf{k}', \mathbf{k}+\mathbf{q}} \delta[E_+(\mathbf{k}') - E_+(\mathbf{k})], \quad (15)$$

where  $|U_q|^2 = |2\pi e^2/[\kappa_I(K_s + q)]|^2 \int e^{-2q|z|} n_i(z) dz$  and  $F(\mathbf{k}', \mathbf{k}) = |\langle \mathbf{k}' | \mathbf{k} \rangle|^2$ .

When a MLBP sheet is placed on a dielectric substrate such as hexagonal boron nitride (HBN) [17], the background impurities in the MLBP layer and the remote impurities in the HBN substrate can contribute to the e-i interaction. Normally, the spacer distance and the concentrations of the remote and background impurities are very hard to determine experimentally. In order to reduce the fitting parameters for the theoretical study, here we assume that

the impurities are effectively located at the interface between the MLBP sheet and the dielectric HBN substrate with an effective concentration  $n_i$ , i.e.,  $n_i(z) = n_i \delta(z)$ . Thus, we have  $|U_q|^2 = n_i |2\pi e^2/[\kappa_I(K_s + q)]|^2$ .

### F. Anisotropic transport mobility

In this work, we employed the Boltzmann equation as the governing transport equation to study the response of the electrons in the conduction band in MLBP to the applied dc driving electric field. Due to an anisotropic feature of the electronic band structure in MLBP, the electronic transport properties along different directions can be different. Thus, one can apply the external electrical current along different directions and measure the voltage along different directions as well. The semiclassical Boltzmann equation in the presence of an external electrical field  $F_{x/y}$  applied along the  $x/y$

direction is

$$-\frac{eF_{x/y}}{\hbar} \frac{\partial f(\mathbf{k})}{\partial k_{x/y}} = g_s \sum_{\mathbf{k}'} [f(\mathbf{k}')W(\mathbf{k}',\mathbf{k}) - f(\mathbf{k})W(\mathbf{k},\mathbf{k}')], \quad (16)$$

where  $f(\mathbf{k})$  is the momentum-distribution function for an electron at a state  $|\mathbf{k}\rangle$ . It is known that there is no simple and analytical solution to Eq. (16) with the electronic transition rate given by Eq. (15). Hence, we utilize the usual momentum-balance equation derived by multiplying  $g_s \sum_{\mathbf{k}} k_{x/y}$  on both sides of the Boltzmann equation, which results in

$$\frac{eF_{x/y}}{\hbar} n_e = 4 \sum_{\mathbf{k}',\mathbf{k}} (k'_{x/y} - k_{x/y}) f(\mathbf{k}) W(\mathbf{k},\mathbf{k}'), \quad (17)$$

where the relation  $n_e = -g_s \sum_{\mathbf{k}} k_{x/y} \partial f(\mathbf{k}) / \partial k_{x/y}$  has been employed. In this study, we assume that the momentum distribution of an electron can be described by a statistical energy distribution function as  $f(\mathbf{k}) \simeq f[E_+(\mathbf{k}^*)]$ . In the presence of the driving electric field  $F_{x/y}$ , the electron momentum is shifted by the presence of the drift electron velocity so that  $\mathbf{k} \rightarrow \mathbf{k}^* = \mathbf{k} - \nu \mathbf{v}$  with  $\mathbf{v} = (v_x, v_y)$  being the drift electron velocity along different directions and  $\nu = (v_x, v_y) = (m_{xc}, m_{yc}) / \hbar$ . For the case of a weak driving field so that the drift electron velocity is small, the energy distribution function can be expanded as

$$f[E_+(\mathbf{k} - \nu \mathbf{v})] \simeq f[E_+(\mathbf{k})] - [\nu_x v_x \partial E_+(\mathbf{k}) / \partial k_x + \nu_y v_y \partial E_+(\mathbf{k}) / \partial k_y] f'(X)|_{X=E_+(\mathbf{k})}.$$

Using the definition of electronic transport mobility,  $\mu_{xx/yy} = -v_{x/y} / F_{x/y} = e\tau_{x/y} / m_{x/y}$ , we get the momentum relaxation time along different directions as

$$\begin{aligned} \frac{1}{\tau_{x/y}} &= -\frac{1}{2\pi^3 \hbar n_e} \\ &\times \int_0^{2\pi} \int_0^{2\pi} \frac{d\phi d\phi' Z_{x/y}}{|\partial h(k',\phi') / \partial k'|_{k'=k'_i} |\partial h(k,\phi) / \partial k|_{k=k_i}} \frac{k'_i(\phi') k_i(\phi) |U_q|^2}{F(\phi',\phi) \left. \frac{\partial E_+(\mathbf{k})}{\partial k_{x/y}} \right|_{(k_x=k_i \cos \phi, k_y=k_i \sin \phi)}}, \quad (18) \end{aligned}$$

where  $q = \sqrt{k'^2 + k_i^2 - 2k'_i k_i \cos \theta}$ ,  $\theta = \phi' - \phi$  is the angle between  $\mathbf{k}'$  and  $\mathbf{k}$ ,  $k_i$  is the  $i$ th solution for  $k$  from equation  $h(k,\phi) = E_+(\mathbf{k}) - E_F = 0$ ,  $Z_x = k'_i \cos \phi' - k_i \cos \phi$  and  $Z_y = k'_i \sin \phi' - k_i \sin \phi$ , and  $F(\phi',\phi) = F(\mathbf{k}',\mathbf{k})$ , in which  $k_x = k_i \cos \phi$ ,  $k_y = k_i \sin \phi$ ,  $k'_x = k'_i \cos \phi'$ , and  $k'_y = k'_i \sin \phi'$ .

For model II, we have  $dE_+(\mathbf{k})/dk_x = \hbar^2 k_x / m_{xc}$  and  $dE_+(\mathbf{k})/dk_y = \hbar^2 k_y / m_{yc}$ ; Eq. (18) then becomes

$$\begin{aligned} \frac{1}{\tau_x} &= -\frac{lm_{xc}}{\pi^2 \hbar^3} \int_0^{2\pi} \int_0^{2\pi} d\phi d\phi' \frac{|U_q|^2 \cos \phi}{g(\phi') g^{3/2}(\phi)} \\ &\times \left( \frac{\cos \phi'}{\sqrt{g(\phi')}} - \frac{\cos \phi}{\sqrt{g(\phi)}} \right) F(\phi',\phi) \quad (19) \end{aligned}$$

and

$$\begin{aligned} \frac{1}{\tau_y} &= -\frac{lm_{xc}^2}{\pi^2 \hbar^3 m_{yc}} \int_0^{2\pi} \int_0^{2\pi} d\phi d\phi' \frac{|U_q|^2 \sin \phi}{g(\phi') g^{3/2}(\phi)} \\ &\times \left( \frac{\sin \phi'}{\sqrt{g(\phi')}} - \frac{\sin \phi}{\sqrt{g(\phi)}} \right) F(\phi',\phi), \quad (20) \end{aligned}$$

where  $g(\phi) = \cos^2 \phi + (m_{xc}/m_{yc}) \sin^2 \phi$ . Here, we should note that  $k_i = \sqrt{t/g(\phi')}$ ,  $k'_i = \sqrt{t/g(\phi')}$ , where  $t = 2\pi n_e l$  with  $l = m_{xc}/m_d$ , and  $q = [t/g(\phi') + t/g(\phi) - 2t \cos \theta / \sqrt{g(\phi')g(\phi)}]^{1/2}$ .

### III. NUMERICAL RESULTS AND DISCUSSION

In the numerical calculations, the band parameters  $\alpha_{c/v}$ ,  $\beta_{c/v}$ , and  $\gamma$  in Eqs. (5) and (6) for MLBP can be determined by using the known effective electron masses and band gaps for ML and bulk BP. In case of bulk BP, the band gap  $E_g = 0.3$  eV [22]; the effective electron masses in different bands and along different directions were determined by the cyclotron resonance measurement [23], which are  $M_{xc} = M_{xv} = 0.08m_0$ ,  $M_{yc} = 1.0m_0$ , and  $M_{yv} = 0.6m_0$  [23], with  $m_0$  being the rest electron mass. At present, these material parameters for MLBP have not yet been determined experimentally. However, the effective electron masses for FLBP have been measured experimentally [25]. Moreover, the results obtained from *ab initio* calculations [24] suggest an energy gap  $E_g = 2$  eV for MLBP [24]. Hence, in the present study, we take the data from experimental results [25] and theoretical calculation [24] to determine the band parameters for MLBP. The effective electron masses  $m_{xc} = m_{xv} \simeq 0.2m_0$  for MLBP can be obtained from the relations  $m_c = \sqrt{m_{xc} m_{yc}}$  and  $m_v = \sqrt{m_{xv} m_{yv}}$ , where  $m_{yc} = M_{yc} = 1.0m_0$  and  $m_{yv} = M_{yv} = 0.6m_0$  are the same as those for bulk BP [27] and  $m_c = 0.47m_0$  and  $m_v = 0.34m_0$  are obtained from magnetotransport measurements via Shubnikov–de Haas oscillations [25] for FLBP. The effective electron masses  $m_{xc}$  and  $m_{xv}$  that we obtain here are a bit larger than those used in the previous work [26] where  $m_{xc} = m_{xv} \simeq 0.15m_0$  were obtained from the *ab initio* calculations [27]. It should be noted that the effective electron masses used in the present study are mainly based on published experimental results. In this study, we consider an air/MLBP/substrate system. We take the dielectric constants for air, bare MLBP sheet, and bare HBN substrate to be respectively  $\kappa_{AIR} = 1$ ,  $\kappa_{BP} = 10.2$  [19], and  $\kappa_{HBN} = 5.1$  [28]. Considering the mismatch of the dielectric constants at the MLBP/HBN interface, we evaluate the effective dielectric constants for MLBP,  $\kappa$ , and substrate,  $\kappa_I$ , from the bare dielectric constants using the mirror image method [29]. Thus we have  $\kappa = (\kappa_{AIR} + \kappa_{HBN})/2 = 3.05$  for electrons in the BP layer and  $\kappa_I = (\kappa_{BP} + \kappa_{HBN})/2 = 7.65$  for impurities in the substrate.

We would like to note that at present, some of the material parameters (e.g., the band gap and the effective electron masses in different bands and along different directions) for MLBP are not well known from direct experimental measurements. Thus, to determine these parameters theoretically we need help from other theoretical calculations and from related indirect experimental results. For example, we take the value of the band gap for MLBP obtained from *ab initio* calculation and calculate the effective masses for MLBP on the basis of experimental data for FLBP. Although the *ab initio* calculation are a CPU-consuming approach, once the band gap is determined from this approach it can be applied for other calculations. The approach employed in this study has a complete theoretical framework. First, the  $\mathbf{k} \cdot \mathbf{p}$  model is applied to obtain analytically the electronic energy spectrum

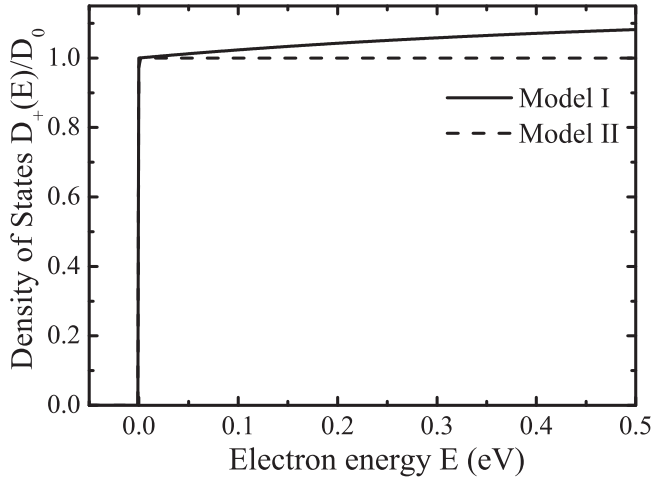


FIG. 1. The density of states  $D_+(E)$  for electrons in MLBP as a function of electron energy  $E$ . The solid and dashed curves represent the results obtained from model I and model II, respectively. Here  $D_0 = m_d/(\pi\hbar^2)$ .

and wave function. In such a calculation the band parameters have to be applied. Second, with the obtained energy spectrum and wave function, the momentum-balance equation derived from the Boltzmann equation is employed to calculate the electron mobility of MLBP at low temperatures. Therefore, once the material parameters such as band gap and electron masses are identified, the proposed theoretical approach can work and simple and CPU-saving calculations are desirable. Furthermore, it is known that the  $\mathbf{k} \cdot \mathbf{p}$  model is valid for the calculation of the electronic states near the bottom of the conduction band and the top of the valence band. Since the present study examines the electronic and transport properties induced by electronic transition near the Fermi level, the standard  $\mathbf{k} \cdot \mathbf{p}$  model is therefore a suitable approach.

In Fig. 1, we plot the DOS for electrons in MLBP as a function of electron energy  $E$ . We can see that the DOS  $D_+(E)$  only exists when electron energy  $E > 0$  for both model I and model II, noting that we have taken the reference energy from the bottom of the conduction band. The results for model II,  $D_+(E) = D_0\Theta(E)$ , show a steplike structure which is similar to that for a semiconductor-based 2DEG system with parabolic subband structure. The DOS given by Eq. (7) for model I (solid curve) is larger than  $D_0$  over all allowed electron energy regimes. This reflects the fact that model I corresponds to a nonparabolic electronic band structure. However, we notice that the difference of the electronic DOS obtained from model I and model II is not significantly big, especially in the low-energy regime.

In Fig. 2(a) we show the Fermi level  $E_F$  as a function of electron density  $n_e$  for MLBP. When the number of electrons increases in an electronic system, the electrons occupy the lower energy states first then the higher energy level. Thus, with increasing electron density  $n_e$ , the Fermi level  $E_F$  increases. As we can see from Fig. 2(a), the difference of the Fermi levels determined from model I (solid curve) and model II (dashed curve) is very little. Consequently, model II can be applied to calculate rightly the Fermi energy for electrons in MLBP.

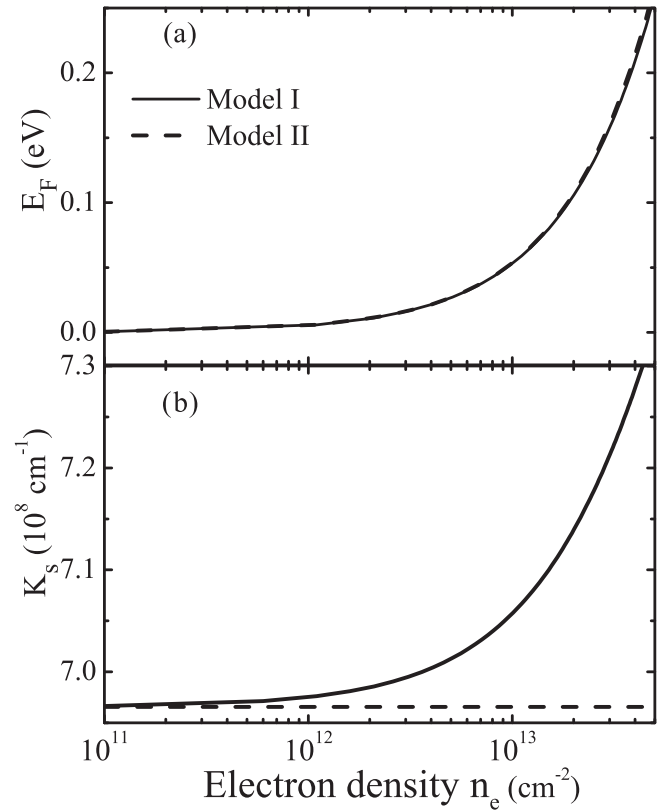


FIG. 2. The Fermi energy  $E_F$ , in (a), and the inverse screening length  $K_s$ , in (b), as a function of electron density  $n_e$ . The solid and dashed curves represent the results from model I and model II, respectively.

In Fig. 2(b), we plot the inverse screening length  $K_s$  obtained from model I (solid curve) and model II (dashed curve) as a function of electron density. The results obtained from model I show that due to the nature of the RPA approach and to a nonparabolic electron energy spectrum, the stronger electronic screening effect can be achieved with increasing electron density. This is in line with the electronic screening effect found in graphene [20]. As shown by Eq. (12), at the  $T \rightarrow 0$  and  $q \rightarrow 0$  limits the RPA inverse screening length  $K_s$  obtained from model II is independent of the electron density. This was also found by previous research work [15,21]. We notice that in the low electron density regime (i.e., when  $n_e < 10^{13} \text{ cm}^{-2}$ ), the difference of  $K_s$  obtained from two models is not significant. Therefore, the simplified model II can describe rather rightly the electronic screening effect for the case of relatively low electron density. It should be noted that  $K_s$  for MLBP has a magnitude of  $10^8 \text{ cm}^{-1}$ , as shown in Fig. 2(b). As we know, for semiconductor-based 2DEG systems,  $K_s$  is often of the order of  $10^7 \text{ cm}^{-1}$  [30]. This is mainly induced by a fact that  $K_s$  is proportional to the DOS electron mass, namely  $K_s \sim m_d$ , as shown by Eq. (12). For MLBP  $m_d = 0.47m_0$ , whereas for semiconductor-based 2DEG (i.e., InAs or GaAs based)  $m_d = 0.04m_0$  or  $0.065m_0$ .

In Fig. 3, the results of electron transport mobility in MLBP along different directions,  $\mu_{xx/yy}$ , are shown as a function of electron density at a fixed impurity concentration  $n_i = 8.85 \times 10^{12} \text{ cm}^{-2}$ . Here we compare the results obtained

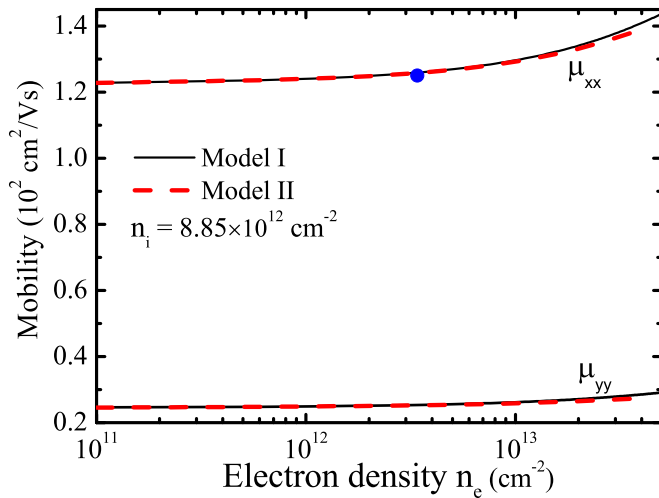


FIG. 3. The electron transport mobilities,  $\mu_{xx}$  and  $\mu_{yy}$ , as a function of electron density at a fixed impurity concentration  $n_i = 8.85 \times 10^{12} \text{ cm}^{-2}$ . The black and red curves represent the results obtained from model I and model II, respectively. The blue dot for  $\mu_{xx}$  is the corresponding experimental result [17].

from two band structure models and from experimental measurement [17]. We note the following points. (i) A strong anisotropic feature of electron transport mobility along different directions can be found. Because  $m_{xc}$  is lighter than  $m_{yc}$ ,  $\mu_{xx}$  is always larger than  $\mu_{yy}$ . (ii) With increasing electron density  $n_e$ , both  $\mu_{xx}$  and  $\mu_{yy}$  increase. This indicates that the application of the gate voltage on MLBP can improve the electron mobility of the sample device. In fact, such experimental measurements have been conducted for FLBP-based field-effect-transistor (FET) devices [6]. (iii) The results obtained from model I and model II for both  $\mu_{xx}$  and  $\mu_{yy}$  are almost identical. This implies that the simplified band structure model can describe rightly the electron mobilities along different directions in MLBP. (iv) When the effective impurity concentration is taken as  $n_i = 8.85 \times 10^{12} \text{ cm}^{-2}$ , the electron mobility  $\mu_{xx}$  from models I and II is at about  $125 \text{ cm}^2/\text{Vs}$  for  $n_e = 3.4 \times 10^{12} \text{ cm}^{-2}$ . This value agrees with the experimental result  $\mu_{FE} = 125 \text{ cm}^2/\text{Vs}$  measured for electrons in a FLBP-based FET device at  $n_e = 3.4 \times 10^{12} \text{ cm}^{-2}$  and  $T = 30 \text{ K}$  [17], shown as a blue dot in Fig. 3.

To show how impurity concentration affects the electron mobility in  $n$ -type MLBP, in Fig. 4 we plot the electron transport mobility along different directions as a function of electron density for different impurity concentrations. Here the results are presented by using model I alone. As for the usual case, both  $\mu_{xx}$  and  $\mu_{yy}$  decrease with increasing impurity concentration  $n_i$  because a larger  $n_i$  leads to a stronger e-i scattering strength. In this study, only one fitting parameter,  $n_i$ , is applied to calculate the electron mobility in MLBP and good agreement with experimental data can be achieved (see Fig. 3).

We note that currently the experimental and theoretical studies of electronic and transport properties of  $p$ -type FLBP have been well conducted. Experimentally, it was found [31] that the hole mobility increases from  $2.0 \times 10^4 \text{ cm}^2/\text{Vs}$

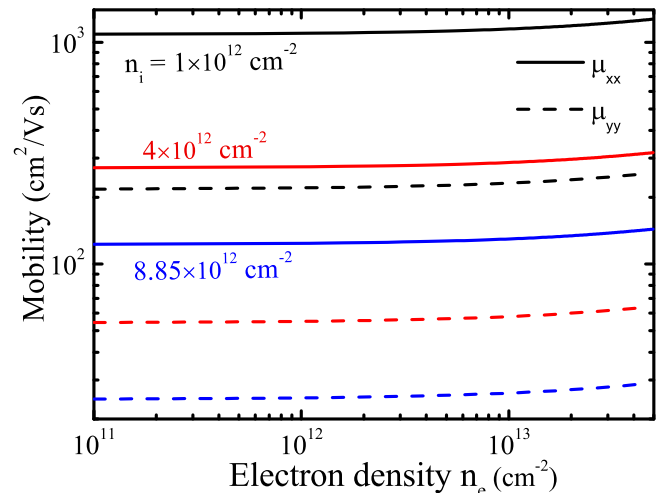


FIG. 4. The electron transport mobilities,  $\mu_{xx}$  (solid curves) and  $\mu_{yy}$  (dashed curves), as a function of electron density  $n_e$  for different impurity concentrations  $n_i$  as indicated.

to  $2.5 \times 10^4 \text{ cm}^2/\text{Vs}$  as the hole density varies from  $2.8 \times 10^{12} \text{ cm}^{-2}$  to  $5.6 \times 10^{12} \text{ cm}^{-2}$  at  $T = 2 \text{ K}$ . Theoretically, it was predicted [15] that the impurity-limited low-temperature mobility for holes in MLBP is of the order of  $10^2 - 10^3 \text{ cm}^2/\text{Vs}$  as the hole density varies in the range of  $10^{12} - 10^{13} \text{ cm}^{-2}$ . The results obtained from this study for electron mobility in MLBP indicate that for both  $p$ -type and  $n$ -type MLBP, the mobility increases with carrier density. We would like to point out that the employed theoretical approach in this study can be applied to calculate the hole mobility in  $p$ -type MLBP as long as the valence band is considered and the related effective hole masses are taken. In Ref. [15], the electronic band structure was taken as the same as our model II but with different hole masses along different directions, and the hole mobility was calculated on the basis of the Boltzmann equation using the relaxation time approximation. From a theoretical point of view, the main difference between the relaxation time approximation [15] and the momentum-balance equation used here is the order to take the average over  $\mathbf{k}$ . Therefore, generally two approaches can lead to very much the same results.

#### IV. CONCLUDING REMARKS

In this work, we have developed a simple theoretical approach to evaluate the basic electronic and transport properties of  $n$ -type MLBP at low temperatures. We have taken two electronic band structure models into consideration. The electron density of states, the Fermi level, the inverse screening length, and the electron transport mobility along different directions have been examined. The main conclusions from this study are summarized as follows.

The simplified band structure model (model II) can be applied to study the electronic and transport properties for  $n$ -type MLBP in the low-energy and low-electron-density regime. Normally, the electron density in FLBP systems is less than  $5 \times 10^{12} \text{ cm}^{-2}$  [6,17]. As a result, the simplified band structure is good enough for studying of the physical

properties of  $n$ -type BP, instead of using a rather complicated energy spectrum for model I.

By taking into account electron-impurity scattering in  $n$ -type MLBP, the electron mobility along the armchair and zigzag directions has been obtained by using the momentum balance equation approach on the basis of the Boltzmann equation. We have examined the dependence of the electron mobility along different directions on electron density and impurity concentration at low temperatures. It has been found that (i) model I and model II can lead to almost identical results; (ii) the anisotropic feature of electron transport mobility along different directions can be observed; and (iii) the good agreement between experimental and theoretical results can be achieved via taking the impurity concentration as the sole fitting parameter for numerical calculation.

The investigation of atomically thin electronic systems (such as graphene and few-layer black phosphorus) has become an important and fast-growing field of research in recent years. We hope the results and discussions presented in this work can help us to gain an in-depth understanding of the basic electronic and transport properties of atomically thin BP materials.

## ACKNOWLEDGMENTS

This work was supported by the National Natural Science Foundation of China (Grants No. 11574319, No. 11304316, No. 11304317, and No. 11604380), the Ministry of Science and Technology of China (Grant No. 2011YQ130018), the Department of Science and Technology of Yunnan Province, and the Chinese Academy of Sciences.

## APPENDIX: THE MATHEMATICAL FORMULAS

In this study, for using model I we need to determine  $k_i(\phi)$  the  $i$ th solution for  $k$  from an equation  $h(k, \phi) = E - E_+(\mathbf{k}) = 0$  with  $\phi$  being the angle between  $\mathbf{k}$  and the  $x$  direction, along with related analytical calculations. From the electron band structure given by Eq. (2), we have that

$$k_i^2 = \frac{-b + \sqrt{b^2 - 4ac}}{2a} \quad (\text{A1})$$

is the solution for  $k$  from  $h(k, \phi) = E - E_+(\mathbf{k}) = 0$ , where

$$\begin{aligned} a &= (A_+ \cos^2 \phi + B_+ \sin^2 \phi)^2 - (A_- \cos^2 \phi + B_- \sin^2 \phi)^2, \\ b &= 2E_g[(A_+ + A_-) \cos^2 \phi + (B_+ + B_-) \sin^2 \phi] + 4E(A_- \cos^2 \phi + B_- \sin^2 \phi) + 4\gamma^2 \cos^2 \phi, \\ c &= -4E(E + E_g), \end{aligned} \quad (\text{A2})$$

with  $A_{\pm} = \alpha_c \pm \alpha_v$ ,  $B_{\pm} = \beta_c \pm \beta_v$ . The partial derivation of  $\partial h(k, \phi)/\partial k$  is given by

$$\begin{aligned} \frac{\partial h(k, \phi)}{\partial k} &= -k(A_- \cos^2 \phi + B_- \sin^2 \phi) - k[(A_+ k^2 \cos^2 \phi + B_+ k^2 \sin^2 \phi + E_g) \\ &\quad \times (A_+ \cos^2 \phi + B_+ \sin^2 \phi) + 2\gamma^2 \cos^2 \phi][(A_+ k^2 \cos^2 \phi + B_+ k^2 \sin^2 \phi + E_g)^2 + 4\gamma^2 k^2 \cos^2 \phi]^{-\frac{1}{2}}. \end{aligned} \quad (\text{A3})$$

The partial derivations of  $E_+(\mathbf{k})$  are given by

$$\frac{\partial E_+(\mathbf{k})}{\partial k_x} = k_x A_- + k_x [(A_+ k_x^2 + B_+ k_y^2 + E_g) A_+ + 2\gamma^2] \times [(A_+ k_x^2 + B_+ k_y^2 + E_g)^2 + 4\gamma^2 k_x^2]^{-\frac{1}{2}}$$

and

$$\frac{\partial E_+(\mathbf{k})}{\partial k_y} = k_y B_- + k_y B_+ (A_+ k_x^2 + B_+ k_y^2 + E_g) \times [(A_+ k_x^2 + B_+ k_y^2 + E_g)^2 + 4\gamma^2 k_x^2]^{-\frac{1}{2}}. \quad (\text{A4})$$

- 
- [1] F. Xia, H. Wang, D. Xiao, M. Dubey, and A. Ramasubramaniam, *Nat. Photon.* **8**, 899 (2014).  
[2] F. H. L. Koppens, T. Mueller, Ph. Avouris, A. C. Ferrari, M. S. Vitiello, and M. Polini, *Nat. Nanotechnol.* **9**, 780 (2014).  
[3] H. Liu, A. T. Neal, Z. Zhu, Z. Luo, X. Xu, D. Tománek, and P. D. Ye, *ACS Nano* **8**, 4033 (2014).  
[4] J. D. Wood, S. A. Wells, D. Jariwala, K. Chen, E. Cho, V. K. Sangwan, X. Liu, L. J. Lauhon, T. J. Marks, and M. C. Hersam, *Nano Lett.* **14**, 6964 (2014).  
[5] R. Fei and L. Yang, *Nano Lett.* **14**, 2884 (2014).  
[6] L. Li, Y. Yu, G. Ye, Q. Ge, X. Ou, H. Wu, D. Feng, X. Chen, and Y. Zhang, *Nat. Nanotechnol.* **9**, 372 (2014).  
[7] C. Q. Han, M. Y. Yao, X. X. Bai, L. Miao, F. Zhu, D. D. Guan, S. Wang, C. L. Gao, C. Liu, D. Qian, Y. Liu, and J. Jia, *Phys. Rev. B* **90**, 085101 (2014).  
[8] M. Buscema, D. J. Groenendijk, S. I. Blanter, G. A. Steele, H. S. J. van der Zant, and A. Castellanos-Gomez, *Nano Lett.* **14**, 3347 (2014).  
[9] Y. Deng, Z. Luo, N. J. Conrad, H. Liu, Y. Gong, S. Najmaei, P. M. Ajayan, J. Lou, X. Xu, and P. D. Ye, *ACS Nano* **8**, 8292 (2014).  
[10] M. Buscema, D. J. Groenendijk, G. A. Steele, H. S. J. van der Zant, and A. Castellanos-Gomez, *Nat. Commun.* **5**, 4651 (2014).  
[11] M. Engel, M. Steiner, and P. Avouris, *Nano Lett.* **14**, 6414 (2014).  
[12] F. Xia, H. Wang, and Y. Jia, *Nat. Commun.* **5**, 4458 (2014).  
[13] E. Flores, J. R. Ares, A. Castellanos-Gomez, M. Barawi, I. J. Ferrer, and C. Sánchez, *Appl. Phys. Lett.* **106**, 022102 (2015).  
[14] A. Jain and A. J. H. McGaughey, *Sci. Rep.* **5**, 8501 (2015).  
[15] Y. Liu, T. Low, and P. P. Ruden, *Phys. Rev. B* **93**, 165402 (2016).

- [16] J. Qiao, X. Kong, Z. Hu, F. Yang, and W. Ji, *Nat. Commun.* **5**, 4475 (2014).
- [17] R. A. Doganov, S. P. Koenig, Y. Yeo, K. Watanabe, T. Taniguchi, and B. Özyilmaz, *Appl. Phys. Lett.* **106**, 083505 (2015).
- [18] Y. Jiang, R. Roldán, F. Guinea, and T. Low, *Phys. Rev. B* **92**, 085408 (2015).
- [19] X. Y. Zhou, R. Zhang, J. P. Sun, Y. L. Zou, D. Zhang, W. K. Lou, F. Cheng, G. H. Zhou, F. Zhai, and K. Chang, *Sci. Rep.* **5**, 12295 (2015).
- [20] H. M. Dong, W. Xu, Z. Zeng, T. C. Lu, and F. M. Peeters, *Phys. Rev. B* **77**, 235402 (2008).
- [21] T. Low, R. Roldán, H. Wang, F. Xia, P. Avouris, L. M. Moreno, and F. Guinea, *Phys. Rev. Lett.* **113**, 106802 (2014).
- [22] A. Morita, *Appl. Phys. A* **39**, 227 (1986).
- [23] S.-i. Narita, S.-i. Terada, S. Mori, K. Muro, Y. Akahama, and S. Endo, *J. Phys. Soc. Jpn.* **52**, 3544 (1983).
- [24] V. Tran, R. Soklaski, Y. Liang, and L. Yang, *Phys. Rev. B* **89**, 235319 (2014).
- [25] L. Li, G. Ye, V. Tran, R. Fei, G. Chen, H. Wang, J. Wang, K. Watanabe, T. Taniguchi, L. Yang, X. Chen, and Y. Zhang, *Nat. Nanotechnol.* **10**, 608 (2015).
- [26] T. Low, A. S. Rodin, A. Carvalho, Y. Jiang, H. Wang, F. Xia, and A. H. Castro Neto, *Phys. Rev. B* **90**, 075434 (2014).
- [27] A. S. Rodin, A. Carvalho, and A. H. Castro Neto, *Phys. Rev. Lett.* **112**, 176801 (2014).
- [28] A. Mogulkoc, Y. Mogulkoc, A. N. Rudenko, and M. I. Katsnelson, *Phys. Rev. B* **93**, 085417 (2016).
- [29] W. Xu, F. M. Peeters, and T. C. Lu, *Phys. Rev. B* **79**, 073403 (2009).
- [30] W. Xu, *Phys. Rev. B* **71**, 245304 (2005).
- [31] G. Long, D. Maryenko, J. Shen, S. Xu, J. Hou, Z. Wu, W. K. Wong, T. Han, J. Lin, Y. Cai, R. Lortz, and N. Wang, *Nano Lett.* **16**, 7768 (2016).